Available online at www.sciencedirect.com
ScienceDirect
Journal of Sound and Vibration 311 (2008) 843–860
JOURNAL OF SOUND AND VIBRATION
www.elsevier.com/locate/jsvi

Acoustic analysis of low-noise actuator design for active flow control

Yueping Guo*

The Boeing Company, Mail Code H013-B308, 5301 Bolsa Avenue, Huntington Beach, CA 92647, USA

Received 24 May 2006; received in revised form 11 July 2007; accepted 25 September 2007
Available online 19 November 2007

Abstract

This paper presents an acoustic analysis of low noise actuation design concepts for active flow control by pulsed jets. The low noise concepts are based on the principle of phase cancellation of coherent unsteady fluctuations. It is shown that by suitably arranging the actuators with prescribed phase variations, active flow control actuators using pulsed jets can achieve very low levels of near-field unsteady fluctuations and far-field noise, while maintaining the same effectiveness in flow control as those conventional designs without the phase cancellation implementation. To demonstrate the concepts, flow separation control on an airfoil is discussed in detail, and numerical simulations are given to show the flow control effectiveness and the low noise features of the actuation design. Simple analytical models are presented to reveal the characteristics of noise radiation from pulsed jet actuators, which relates the near-field pressure and far-field noise to various parameters such as the mean flow Mach number, the frequency of the pulsed jets and the phase variation algorithm. The explicit analytical results can be used as a quick design guide in practical applications.

1. Introduction

In recent years, pulsed jet injection has been shown to be an effective technique in active flow control, including the suppression of boundary layer flow separation on aircraft wings (for overviews, see Refs. [1–3]), and hence, is considered to be a potential technology to improve aircraft performance for both military and civilian applications. For flow separation control on aircraft wings, for example, active flow control has been shown to be able to eliminate flow separation and improve the aircraft lift by as much as 30 percent (e.g., Refs. [4–7]). However, it has also been recognized that the implementation of active flow control in practical applications faces practical issues, some of which may become show stoppers if unresolved. In the case of actuation by pulsed jets, the unsteady pressure fluctuations and the associated noise generated by the pulsed jets can be such a show stopper. The near-field pressure fluctuations are the sources of aeroacoustic loads that can potentially cause acoustic fatigue on the aircraft, significantly affecting the structure design of the aircraft. Effective pulsed jets for active flow control usually operate at frequencies in the 100 Hz range. For example, Bower and Kibens [2] and Ronald et al. [3] both reported effective actuators in this frequency range.

*Tel.: +1 714 896 1527; fax: +1 714 896 1559.
E-mail address: yueping.guo@boeing.com

0022-460X/$ - see front matter © 2007 Elsevier Ltd. All rights reserved.
doi:10.1016/j.jsv.2007.09.053

Nomenclature

A	amplitude of pressure waves
b	half-length of actuator slot
B	far-field noise amplitude
c_0	constant sound speed
C_L	lift coefficient
C_μ	momentum blowing coefficient
f	frequency
f_+	frequency normalized by airfoil chord and mean flow velocity (fU/L)
F	time variation of pulsed jets
G	Green's function
h	half-width of actuator slot
H	Heaviside function
k_0	acoustic wavenumber
k_n	discrete wavenumber of spatial modulation of discrete actuators
K	number of pulsed jet pulsation period
L	airfoil chord length
m	order of harmonics in pulsed jet velocity spectrum
$\mathbf{M}$	mean flow Mach number vector
M	mean flow Mach number magnitude
n	index for actuator array
N	number of pulsed jets in actuator array
p	pressure fluctuation
R_e	Reynolds number
R^*	source to microphone distance modified by flow effects
S	pulsed jet opening area
t	time
T	pulsed jet pulsation period
U	amplitude of mean flow velocity
$\mathbf{V}_0$	amplitude vector of pulsed jet velocity profile
$\mathbf{V}_J$	velocity vector of continuous pulsed jets
$\mathbf{V}_n$	velocity vector of discrete pulsed jets
V_J	amplitude of pulsed jet velocity
$\mathbf{x}$	microphone location coordinates
$\mathbf{y}$	source (pulsed jets) coordinates
α	angle of attack
β	quantity related to mean flow Mach number
θ	far-field polar angle
ϕ	far-field azimuthal angle
φ	phase of pressure waves (with subscript 1 or 2)
η	design parameter controlling the noise reduction
ℓ	separation distance of individual jets in actuator array
ρ_0	mean flow density
τ	time delay
τ_n	time delay of individual pulsed jets
ω	angular frequency of pulsed jets

It is in this low frequency range that the aircraft structure is most likely to couple to the flow excitation through resonance responses, potentially causing severe acoustic fatigue. The noise radiated in the surrounding environment by the pulsed jets can also be a potential environmental hazard, potentially exposing the general population community and/or the ground or deck crew to noise pollution. Though the operating frequency of the pulsed jets is usually low, at the low end of the audible frequency range for human ears, the rich harmonics of the pulsed jet spectrum can excite tones in a much wider frequency domain, covering both the low and the high frequency range.

All these undesirable effects can occur in practical applications, depending on parameters such as the pulsating frequency of the actuators, the amplitude of jet velocity and the number of actuator jets in the application. To avoid and/or mitigate these effects, it is clearly desirable to have actuator design strategies that have significantly low levels of unsteady pressure fluctuations and noise, but are still able to achieve the control effectiveness in enhancing the aerodynamic performance of the vehicle. This is what has motivated the study reported here; we will discuss pulsed jet actuation designs that achieve the dual objective of low noise generation and effective flow control.

The principles for achieving this dual objective are the two different physical mechanisms, respectively, in the linear and nonlinear flow regime. For flow control, it is the high intensity momentum/energy injected into the flow that alters the flow characteristics, a phenomenon that is related to nonlinear quantities proportional to the square of the flow velocity. For low noise radiation, the physical mechanism relies on the superposition principle of acoustic waves, making use of the additive feature of linear acoustic waves, a feature that enables mutual cancellation between coherent waves of different phases and has seen successful applications in various

areas (e.g., Refs. [8–11]). When the phase differences are suitably arranged, significant mutual cancellation between the waves can occur, yielding resultant amplitudes that are much smaller than any of the individual waves. This cancellation mechanism can be implemented by spatially modulating a time delay in the pulsed jet velocity pulsations, equivalent to introducing phase variations in the acoustic waves.

Since these two mechanisms work in different flow regimes, they can coexist and can both be effective. This will be demonstrated in detail by the case of flow separation control on airfoils, which apparently has applications in aircraft wings, as well as rotorcraft blades and other applications. For this purpose, numerical simulations will be performed for an airfoil in a subsonic mean flow at an angle of attack of 18°, for which case, flow separation is inevitable without active flow control. It will be shown that the flow separation can be effectively suppressed by pulsed jet injection with spatially modulated time delays in the pulsating jet velocity. The aerodynamic performance of the airfoil in this case will be shown to be at least as good as the case with spatially uniform pulsed jet control, which establishes the flow control effectiveness of the low noise designs.

To reveal the low noise features of the actuation strategies with time delays in the jet pulsation, we will develop simple analytical models for the jet pulsation velocity, and the induced near-field pressure fluctuations and the far-field noise. Analytical models for the acoustic analysis are feasible in this particular application because of the low mean flow Mach number and the relatively smooth geometry in the region where the actuators are located, usually in the middle chord region on the smooth upper surface of the airfoil which is also the region where flow separation usually starts; the radiation from the actuators resembles that of a piston on a large wall with prescribed velocity distribution. The prediction of the total radiation in the far field will of course have to be determined by including the reflection by the airfoil, as well as the diffraction by its leading and trailing edges, but those effects can be expected to be of second order in the study of the acoustic radiation characteristics of the pulsed jets, especially when their low noise designs are the primary topic. The direct radiation from the jets, which is modeled analytically here, is very likely to be the main contribution to the total noise. The analytical models will clearly reveal the radiation characteristics of the pulsed jets, both in spectral features and in functional dependencies on flow and geometrical parameters. The former includes the generation of tones by the harmonics of the jet velocity spectrum, which, for uniform pulsation actuators without considerations of low noise design, can have non-negligible amplitudes and cover almost the entire frequency domain for human ear reception, as well as the low operation frequencies of jets. It is this rich tonal structure of the jet radiation that may become practical issues for both acoustic fatigue and environmental noise. These issues can be mitigated by the low noise design, and the analytical models studied here will show that both the near-field pressure fluctuations and the far-field noise from the pulsed jets can be minimized to insignificant levels. Simple formulas will be derived that related the low noise radiation to design parameters of the jet actuators, which can be used as quick guidelines in practical applications.

2. Low noise design concepts

In active flow control, pulsed jets are commonly used as actuators and have been shown to be effective in achieving the flow control objectives. The low noise actuation design discussed here follows this successful strategy, but differs from conventional designs by using spatially modulated pulsation for implementing the control jets. This spatially modulated design gives time delays, corresponding to phase variations in frequency domain, between segments of the actuator or between individual elements of an array of actuators, which can be utilized to minimize the noise radiated from the actuators. Apparently, such a design needs to be shown to be effective in both low noise radiation and flow control, which will be discussed in detail in the following sections. In this section, we introduce the concept of this low noise design, describe how the spatial modulation can be implemented and explain the principles of low noise radiation for these designs.

The spatial modulation of pulsed jet actuators can be achieved in many ways and two examples are shown in Figs. 1 and 2, both for the case of flow separation control on aircraft wings. Depending on the design of the actuators, the spatial modulations can be either continuous or discrete. Fig. 1 shows an actuator in the form of a long slot on an aircraft wing. In this case, the spatial modulations can be implemented by a continuously varying jet velocity, along the length of the slot and as a function of time. The practical implementation of continuously varying jet velocity is by no mean trivial, but is certainly feasible. For example, the continuously varying jet may be formed by an array of individual jets inside the blowing chamber, operating with different

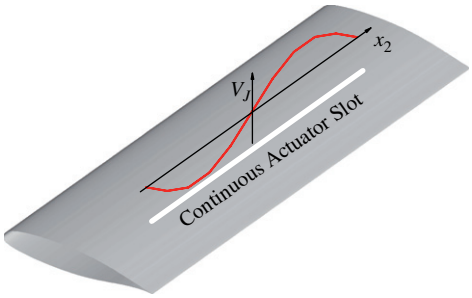

Fig. 1. Wing with a continuous pulsed jet slot for active flow control with spatially modulated jet velocity for low noise operations.

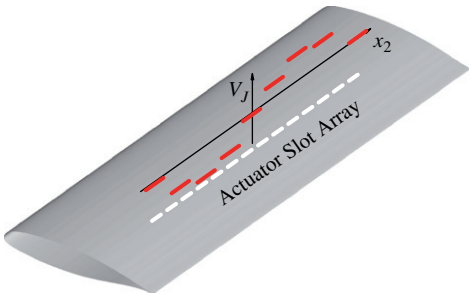

Fig. 2. Wing with an array of slot-shaped pulsed jets for active flow control with time-delayed pulsation for low noise operations.

velocities. The individual jets of different velocities will mix with each other to form a continuously varying jet, flowing out of the long slot. In cases where it is not necessary to have a continuous jet actuator, Fig. 2 shows the case of an array of actuators in the form of individual jets. In this case, the jet velocity spatial modulation is in the form of variations between the individual jets. In general, the jet pulsation is periodic and its velocity can be described by

$$\mathbf{V}_J = \mathbf{V}_0 F(t), \tag{1}$$

where $\mathbf{V}_J$ denotes the pulsed jet velocity vector, whose time variations are specified by the scalar function F as a function of time t, and $\mathbf{V}_0$ is the amplitude vector of the jet velocity, which in practical applications can have three components. For low noise design, we introduce a time delay to the pulsed jet, which is denoted by τ and is a function of the spatial coordinates of the jet actuators. Thus, we replace Eq. (1) by

$$\mathbf{V}_J = \mathbf{V}_0 F(t + \tau(\mathbf{x})). \tag{2}$$

Here, $\mathbf{x} = (x_1, x_2, x_3)$ is the coordinates set such that the free stream flow is in the x_1 direction, x_2 is the span-wise direction, which is also the length direction of the actuator slot, and x_3 is the transverse direction. For the continuous slot actuator shown in Fig. 1, the time delay can be set to

$$\tau = \eta x_2 / c_0 \tag{3}$$

which varies with the span-wise spatial coordinate x_2 in the direction of the slot length, where c_0 is the constant sound speed and η is a non-dimensional free design parameter, the value of which can be determined by the minimum amount of noise radiation allowed for a given actuator design. In general, larger values of η give better acoustic performance. However, larger values of η also mean rapid spatial variations of the pulsed jet velocity, which may not be easy to implement in practical applications. Thus, the choice of η can be made by balancing the need for low noise radiation and the practical limitations of implementing the actuator system. Note that if this parameter is set to zero, the definition Eq. (2) recovers the case of uniform pulsed jet.

For discrete actuators such as arrays of small pulsed jets illustrated in Fig. 2, the continuous spatial modulations specified by Eqs. (2) and (3) can be replaced by

$$\mathbf{V}_J = \mathbf{V}_n = \mathbf{V}_0 F(t + \tau_n), \tag{4}$$

where $\mathbf{V}_n$ is the velocity of the nth jet, $n = 1, 2, 3, \ldots, N$, with N denoting the total number of actuators in the pulsed jet array, and the time delay between the individual jets in the actuator system is now implemented by the discrete time delay factor τ_n, given by

$$\tau_n = \eta n \ell / c_0, \tag{5}$$

where ℓ is the distance between two neighboring actuators. For discrete actuator jets like this, the pulsed jet velocity distributions are illustrated in Fig. 2. This can be regarded as a snapshot for some particular choices of the design parameter η, which, again, needs to be chosen by balancing the low noise requirement and the practical feasibility of the implementation of the actuator systems (the number of jets, for example). The figure shows the case of an actuator array of short slots, but the pulsed jet velocity distribution Eq. (4) also holds for arrays of other actuator shapes. For example, circular shaped pulsed jet actuators are a convenient choice in practical applications.

The time delays introduced by Eqs. (2) and (4) in the pulsed jet velocity correspond to phase variations in frequency domain. This becomes clear once the time domain jet velocity variation is transformed into frequency domain, according to the definition

$$\tilde{F}(\omega) = \int_t F(t)\, \mathrm{e}^{\mathrm{i}\omega t}\, \mathrm{d}t \quad \text{and} \quad F(t) = \frac{1}{2\pi} \int_\omega \tilde{F}(\omega)\, \mathrm{e}^{-\mathrm{i}\omega t}\, \mathrm{d}\omega, \tag{6}$$

where ω is the angular frequency and the overhead tilde denotes quantities in the Fourier transform domain. When Eq. (6) is applied to Eq. (2), the left-hand side gives the Fourier transform of the jet velocity vector. For the right-hand side, the transform of the scalar function F at the delayed time $t + \tau$ can be facilitated by making use of the shift theorem of Fourier transform. This leads to

$$\tilde{\mathbf{V}}_J(\omega) = \mathbf{V}_0 \tilde{F}(\omega)\, \mathrm{e}^{-\mathbf{i}\omega\tau(\mathbf{x})} = \mathbf{V}_0 \tilde{F}(\omega)\, \mathrm{e}^{-\mathbf{i}k_0 \eta x_2}, \tag{7}$$

where the last step follows from the use of Eq. (3) for the time delay factor and we have introduced the acoustic wavenumber $k_0 = \omega/c_0$ to save writing. This result shows that the time delay gives each frequency component a different phase.

The time delay rules specified by Eqs. (3) and (5), respectively, for continuous and discrete pulsed jets, are designed so that the unsteady pressure waves from the individual segments of the continuous slot-jet, or the individual jets in an actuator array, are generated with different time delays or different phases. The delay rules are determined by the geometry of the actuators, the number of jets, the arrangement of the array and the frequency of the pulsation. The pressure fluctuations from each individual segment or each individual jet have peaks and valleys at different times. Thus, the total pressure fluctuations, which are the instantaneous summation of the individual components, can be much smaller than the individual components if the individual components destructively interfere with each other, leading to the canceling or offsetting effects of the individual peaks and valleys in the pressure waves. This results in much lower levels of the unsteady pressure fluctuations than the cases without spatial modulations where the waves are in phase and their peaks and valleys enforce each other. This is of course the well-known principle of phase cancellation for coherent linear waves. It has been known for a long time and has been well utilized in technologies such as active noise and vibration control (e.g., Refs. [8,9]).

3. Active flow control simulation

In designing low noise actuators for active flow control, it is crucially important to first make sure that the low noise features do not affect the effectiveness of the actuators in their functions of flow control. From the physical mechanisms of phase cancellation discussed in the previous section, the spatial modulations can lead to low levels of noise radiation. It then remains to ensure that the phase cancellation between the individual jet segments or individual jets do not cancel the effects of flow control from each other, which is the focus of this section.

Before we present the detailed numerical simulation, it is instructive to discuss, from the physics of active flow control, whether the low noise actuation design by spatial modulation would have any adverse effects in the effectiveness of the actuators in achieving the flow control objective. The mechanism of active flow control

by pulsed jets utilizes the injection of high intensity momentum and energy into the base flow, energizing the flow so that flow separation is delayed or suppressed. By definition, flow momentum and energy are nonlinear quantities, proportional to the square of linear quantities such as the jet velocity and the induced pressure fluctuations. The aggregate effects of flow control by pulsed jets are determined by the total momentum and energy injection, which is the summation of the contributions from individual segments of continuous actuators or individual elements of actuator arrays. Since this is a summation of nonlinear quantities, it can be conjectured that the phase information of the linear quantities is not relevant and does not affect the total, similar to the incoherent summation in acoustics. Thus, it can be expected that the spatial modulation of the linear quantities does not have any significant effect on the flow control. This gives the physical reason why effective flow control and low noise features can both be designed into an innovative actuator concept. The two mechanisms can coexist because they operate in different flow regimes. For low noise radiation, the design relies on the linear additive features of pressure waves, and for active flow control, it is the nonlinear momentum and energy injection that modify the flow to achieve the desired control effects.

To demonstrate the effectiveness of the actuator design in achieving both low noise radiation and effective flow control, we discuss an example of flow separation control on airfoils. The geometry is shown in Fig. 1, as an un-swept wing with a long slot on the upper surface of the wing as active flow control actuator. The geometry is a cross section cut of a real aircraft wing [12,13] and is a modified NACA0012 airfoil. The example can be studied by using computational fluid dynamics to simulate the flow field around the airfoil. We choose to use the computational fluid dynamics code OVERFLOW with over set grids, which is convenient in adding local regions of refined grids when control actuators are added to the simulation. The overall grids are the conventional C-type grid, with 413 grids in the streamline direction, 73 in the wing normal direction and 49 in the span-wise direction. The computational domain extends about 13 chord lengths in the upstream direction, 20 chord lengths in the downstream direction, and about 14 chord lengths both above and blow the airfoil. In dimensional units, the airfoil has a chord length of 14 inches and a span of 48 inches. The grids around the airfoil in a span-wise cut are illustrated in Fig. 3, showing the tight cluster both in the trailing edge region and in the location of the flow control actuators, about 40 percent chord length upstream of the trailing edge. This dense grid cluster is designed to capture the effects of the pulsed jets. In the computational fluid dynamics calculation, the ends of the computational domain in the span-wise direction are simulated as inviscid walls to avoid the complexity of airfoil tip grid.

The airfoil operates at an angle of attach of 18° in a subsonic mean flow of Mach number 0.179 with the flow Reynolds number being 1.484 million, based on the free stream velocity and the airfoil chord length. For convenience, the flow conditions, together with the basic dimensions of the airfoil model, are summarized in Table 1. At these conditions, the flow on the upper surface of the airfoil separates, forming a recirculation flow region near the trailing edge of the airfoil on the upper surface side, which is clearly shown in Fig. 4 by the streamlines in the vicinity of the trailing edge. The separation bubble covers about 40 percent of the airfoil chord near the trailing edge region.

As is known in active flow control, separation of this kind can be effectively suppressed by pulsed jet blowing at the onset of the separation bubble. This can be demonstrated by a slot jet actuator located at 40 percent of airfoil chord upstream of the trailing edge on the upper surface. The control jet pulsates at a prescribed frequency of 217 Hz, which leads to oscillating jet velocity of amplitudes

$$\mathbf{V}_J/c_0 = \{0.62, 0, 0.143\} \tag{8}$$

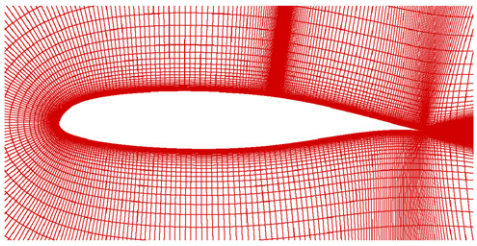

Fig. 3. Illustration of grids used in numerical simulation in the region near the airfoil surface.

Table 1
Flow conditions and airfoil dimensions for computational fluid dynamics simulation

M	α	R_e	Chord	Span
0.179	18°	1.484×10^6	14″	48″

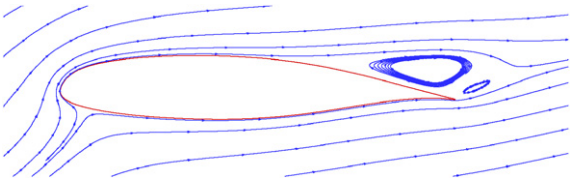

Fig. 4. Streamlines near the airfoil illustrating flow separation on its upper surface, in a subsonic flow at 18° of angle of attack.

which gives the pulsed jet a velocity magnitude of

$$V_J/c_0 = |\mathbf{V}_0|/c_0 = 0.6363. \tag{9}$$

Here, the three components in the jet velocity are the components in the Cartesian coordinates, which are imposed as boundary conditions in the numerical simulations. It should be noted that the control jet can be better simulated as part of the flow, not as boundary conditions, but since our main objective here is to demonstrate the principles of the low noise design, we feel that the simplified actuator simulation is justified. As is conventional in active flow control, the pulsed jet velocity is related to the momentum blowing coefficient C_μ by the definition

$$\langle C_\mu \rangle = (4h/L)\left(\langle V_J \rangle^2/U^2\right), \tag{10}$$

where the bracket $\langle\ \rangle$ denotes quantities associated with root mean squared quantities, h is the half-width of the actuator slot, L is the chord length of the airfoil and U denotes the amplitude of the free stream velocity at infinity. As is commonly known, the root mean squared velocity of a single frequency variation differs from the amplitude of the velocity variations by the factor of the square root of 2. In our notation, this states

$$\langle V_J \rangle = |\mathbf{V}_0|/\sqrt{2}. \tag{11}$$

For the flow separation control discussed here, the slot opening where the high intensity momentum is injected into the boundary layer of the airfoil is 0.32 percent of the airfoil chord length, which leads to a momentum coefficient of 0.0404. The actuator jets pulsate to introduce high intensity flow into the base flow, but the pulsation does not have any spatial variation. Here, the velocity of the jet is much higher than the mean flow, which is what we mean by high intensity flow. The parameters of the control jet are chosen to demonstrate the ideas discussed here and are not meant for any practical applications, though they are all within the practical ranges studied for active flow control. It should be noted that much smaller values of momentum coefficient, of the order of 10^{-4} have been seen to be effective in some cases. The value we use for the demonstration in this paper is consistent with our experimental studies, and is also consistent with that reported in Ref. [2]. For convenience, the geometry and operation conditions of the pulsed jet are summarized in Table 2.

The computational fluid dynamics results with active flow control are illustrated in Fig. 5, again, by the streamlines around the airfoil. Clearly, the large separation bubble is suppressed by the pulsating jet. The benefit of suppressing the flow separation can also be illustrated by the gain in the lift coefficient of the airfoil, which is shown in Fig. 6 where the lift coefficient is plotted as a function of the number of iterations in the numerical calculation, equivalent to time. In the computation, the active flow control is turned on after the baseline uncontrolled case has reached a steady state. Thus, the value of 1.82 for the lift coefficient before the control is turned on is for the case with flow separation. After the control is turned on, Fig. 6 shows that the lift coefficient is increased to the range between 2.22 and 2.44, an average increase of about 28 percent. The oscillations in the lift coefficient are inherent for this kind of conventional pulsation jet actuators, resulting

Table 2
Specifications of the continuous slot pulsed jet actuator for flow separation control

h/L	b/L	C_μ	f	f_+
0.0016	1.1429	0.0404	217 Hz	1.2679

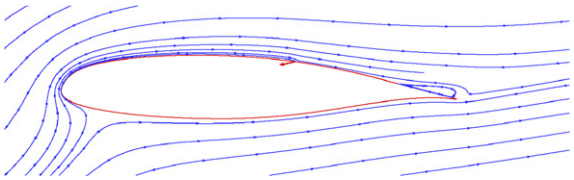

Fig. 5. Streamlines around the airfoil with active flow control, illustrating the suppression of flow separation on its upper surface.

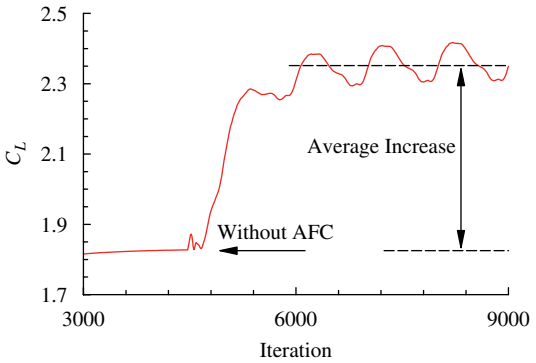

Fig. 6. Illustration of wing lift increase by active flow control with uniform pulsed jet actuators.

from the pulsation of the jets. It is an undesirable feature that implies an unsteady lift experienced by the airfoil on the magnitude of about 10 percent. All these results are well known in active flow control and are repeated here to set the baseline configuration (pulsating jet actuator without spatial modulation) for noise calculation and for comparison with the spatially modulated pulsed jet design.

Having established the baseline configuration, it only remains to show that the actuator design with spatially modulating pulsed jets is at least as effective as the baseline conventional pulse-jet actuator. For this purpose, we repeat the computational fluid dynamics simulation with the same baseline geometry, but with the actuator jet pulsating according to Eq. (2), with the wavenumber parameter η set to unity. Some results of this simulation are shown in Fig. 7, which plots the streamlines at three different span-wise locations. Different span-wise locations are shown here because the actuator jet velocity has span-wise variations due to the spatial modulation and it is important to make sure the active flow control works for the entire wing. In comparison with the uncontrolled case shown in Fig. 5, the flow separation is clearly suppressed by the spatially modulated actuator at all spanwise locations. Similarly to the control with uniform jet pulse, the benefit of the active flow control can be also shown by the lift coefficient of the wing, as plotted in Fig. 8 as a function of the computation iteration number. Before the actuator is turned on, the wing has a large separation on its upper surface and its lift coefficient is about 1.82. With the active flow control, the lift coefficient is increased to about 2.36. It can be noted that the lift coefficient is smooth, in comparison with the oscillatory results for the baseline uniform pulse actuator shown in Fig. 6, and the value of 2.36 is slightly higher than the average of the oscillatory results of 2.33. Both of these can be regarded as small improvements in the effectiveness of the

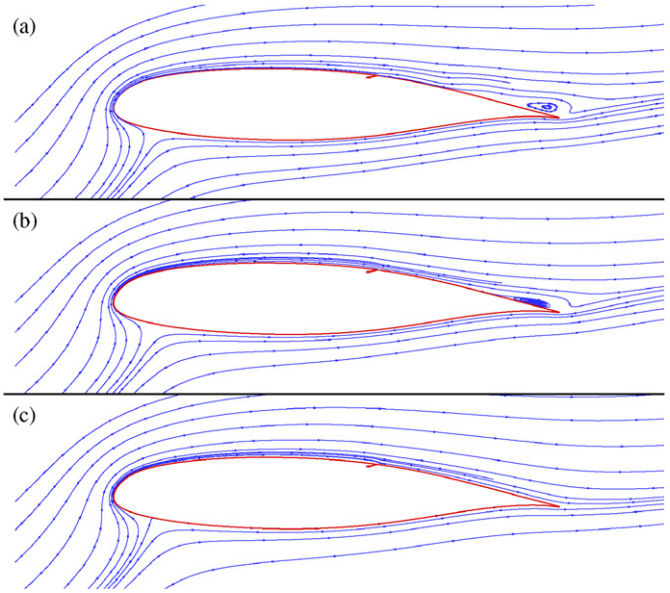

Fig. 7. Streamline plots around the airfoil at various span-wise locations with spatially modulated active flow control: (a) $y = -0.86c$; (b) $y = 0$; and (c) $y = 0.86c$.

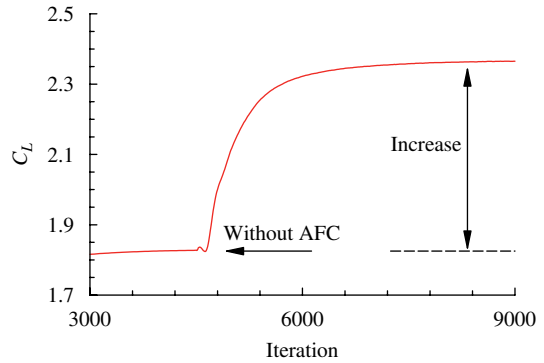

Fig. 8. Lift coefficient of a wing with spatially modulated active flow control.

active flow control actuator due to spatial modulation. However, it is the low noise features that are the significant improvements, which will be discussed in the following sections.

4. Pressure fluctuations from pulsed jets

The unsteady pressure fluctuations induced by the pulsed jet actuators and their noise radiation contain two components, one from the pulsation that induces oscillatory mass injection into the flow and the other due to the turbulent flows both from the jets and from the turbulent boundary flow of the airfoil. The radiation from the latter can be the broadband noise from the turbulence, as well as the scattering of the turbulent eddies by the geometry of the actuators, as analyzed in detail in Refs. [14,15]. Because of the small dimensions of the jet actuators, the turbulence noise can be expected to be smaller than that due to the pulsation of the jets, because the pulsating jets can induce very efficient acoustic sources. Thus, in discussing the acoustic effects of pulsed jet actuators, it is sufficient to consider, as a leading order analysis, the noise radiation from the pulsating flows from the control jets. With the jet velocity defined by formulas such as Eqs. (1) and (3), the radiation can be computed by numerical methods, for example, the method of computational aeroacoustics, which solves the

linear Euler equation for the disturbances produced by the pulsed jet. Computations of this kind are currently feasible, but are by no means trivial, mostly because of the intensive requirements on computer resources. For this reason, we present in this section a simplified analysis on the noise radiation from the pulsed jets. The simplification results from the low Mach number of the mean flow and the simple airfoil geometry. Because of the low Mach number, the mean flow effects can be characterized by a uniform flow, equal to the free stream flow, which neglects all the effects of the boundary layer flows near the airfoil surfaces and the non-uniform effects due to the presence of the airfoil itself. Furthermore, for the airfoil problem considered here, the airfoil surface area surrounding the actuators is relatively flat, so that the effects of the airfoil surface can be approximated by a flat large plate. This approximation neglects the diffraction of the acoustic waves by the trailing and leading edges. Thus, the computed pressure fluctuations can be considered as the direct radiation from the pulsed jets before any interactions with the airfoil geometry. Since this part of the pressure fluctuations is expected to be the most severe, the analysis can be regarded as a leading order analysis, especially for the loading on the airfoil surface near the actuators. Clearly, for the surface pressures on the lower surface of the airfoil and for the far-field noise on the down-side, the diffraction by the airfoil geometry is an important feature that has to be included in the analysis. This can be done by the method of computational aeroacoustics or the boundary element method, which, however, will not be pursued here but be left to a future study.

With the simplifications discussed above, the pressure fluctuations induced by the pulsed jets can be computed in the frequency domain by the simple formula

$$\tilde{p}(\omega,\mathbf{x}) = V_J \tilde{F}(\omega) \int_{S(\mathbf{y})} \mathrm{e}^{-\mathrm{i}\omega\tau(\mathbf{y})} G(\mathbf{x}-\mathbf{y})\,\mathrm{d}s(\mathbf{y}), \tag{12}$$

where $\tilde{p}$ is the induced pressure fluctuation at the location $\mathbf{x}$ and the angular frequency ω, which is given by the pulsed jet velocity distribution V_J and the Green's function G. The integration is over the open areas of the pulsed jet actuators, collectively denoted by S. The Green's function is given by [16]

$$G(\mathbf{x}-\mathbf{y}) = \frac{\rho_0\omega}{2\pi\mathrm{i}R^*\beta^2}\left\{1+\frac{(\mathbf{x}-\mathbf{y})\mathbf{M}}{R^*}\left(1+\frac{\mathrm{i}\beta^2}{k_0R^*}\right)\right\}\mathrm{e}^{\mathrm{i}k_0\left(R^*+\mathbf{M}(\mathbf{x}-\mathbf{y})\right)/\beta^2}. \tag{13}$$

Here ρ_0 is the mean flow density, $\mathbf{M}$ is the vector mean flow Mach number and R^* denotes

$$R^* = \sqrt{\beta^2|\mathbf{x}-\mathbf{y}|^2+((\mathbf{x}-\mathbf{y})\mathbf{M})^2} \tag{14}$$

with β introduced to save writing, defined by

$$\beta^2 = 1-M^2. \tag{15}$$

It can be seen that the Green's function defined by Eq. (13) includes both near-field and far-field contributions; the last term in the bracket in Eq. (13) on the right-hand side is the near-field contribution that becomes negligible in the far field, compared with other terms, but dominates the induced pressure fluctuations in the region in the vicinity of the pulsed jet actuators, and hence, is important in analyzing the aeroacoustic loads on the airfoil surface.

For any given jet velocity distribution $\mathbf{V}_J$, the integration in Eq. (12) can be easily carried out by numerical methods to derive the induced pressure fluctuations in frequency domain. The time domain results can then be easily derived through the inverse Fourier transform defined in Eq. (6). It should be noted that though the pulsed jet velocity is usually considered as periodic, it is not a pure, single frequency variation. On the contrary, because of the rapid rise and fall of the time variations when the jet velocity changes sign, the pulsed jet velocity spectrum contains many frequencies, in the form of harmonics to the prime pulsating frequency, and the harmonics can generate tones in the induced pressure fluctuations and the radiated far-field noise of significant amplitudes. Thus, in studying noise radiation from active control pulsed jet actuators, it is important to consider all frequency components.

The spectral features of pulsed jet velocity can, in fact, be studied and understood by analytical examples. The velocity profile in time domain is approximately of box-type, maintaining positive constant amplitude for half of the period and then rapidly changing to negative constant amplitude for the other half of the pulsating

period. Thus, the time variations of the pulsed jet velocity can be modeled as

$$F(t) = \sum_{k=1}^{K} \{H(t-(k-1)T) - 2H(t-(k-1/2)T) + H(t-kT)\}, \tag{16}$$

where the summation of k is over all the periods of pulsed jet operation, denoted by K, and the symbol H is the Heaviside function, equal to unity for positive arguments and zero otherwise. This analytical function defines a periodic pulsation. Within each period, the function is equal to unity for the first half-period and equal to negative unity for the second half. It should be pointed out that this analytical expression is used here only for the purpose of understanding the features of periodic pulse jets. In practical implementation and numerical simulations, the jet velocity profile is usually smooth. It is easy to show that the Fourier transform of this analytical function is simply

$$\tilde{F}(\omega) = \frac{1}{\mathrm{i}\omega}(1 - \mathrm{e}^{-\mathrm{i}\omega T/2})^2 \sum_{k=1}^{K} \mathrm{e}^{\mathrm{i}\omega kT}. \tag{17}$$

The induced pressure fluctuations given by Eq. (15) also show frequency dependence in the surface integration, resulting from the Green's function defined by Eq. (16). However, since the jet velocity spectrum is strongly dominated by the sharp tones in the jet velocity spectrum, the induced pressure spectrum will also be dominated by these tones. Thus, it is sufficient to only analyze the result Eq. (12) at these discrete frequencies. Clearly, the pressure fluctuations also depend on the mean flow Mach number, the size and geometry of the actuator and the amplitude of pulsed jet velocity. The functional dependencies on these parameters may vary with the microphone location; whether the microphone is in the near or far field of the pressure fluctuation waves, for example. For applications of acoustic fatigue and aeroacoustic loads, it is the near-field results that are of interests. For the baseline case of a slot pulsed jet with uniform velocity along the slot, the pressure fluctuations are shown in Fig. 9 for the primary pulsation frequency and its first three odd integer harmonics. The figure plots the pressure levels in decibels on the upper surface of the wing, where the jet actuator is located. The pressure levels plotted in this figure, and in subsequent similar plots, are normalized according to

$$20 \log |\tilde{p}(\omega)/(\rho_0 c_0 L)|, \tag{18}$$

where L denotes the airfoil chord length. All the flow and geometry parameters are the same as those given in the previous section, as summarized in Tables 1 and 2. As expected, the high levels of the pressure fluctuations occur in regions close to the jet actuator and the spatial distribution depends on the pulsating frequency. It can be seen from Fig. 9 that the pressure level distributions for the tones have different spatial patterns and the patterns for the higher order tones show clearly lower levels. This decreasing trend of the tone amplitudes with

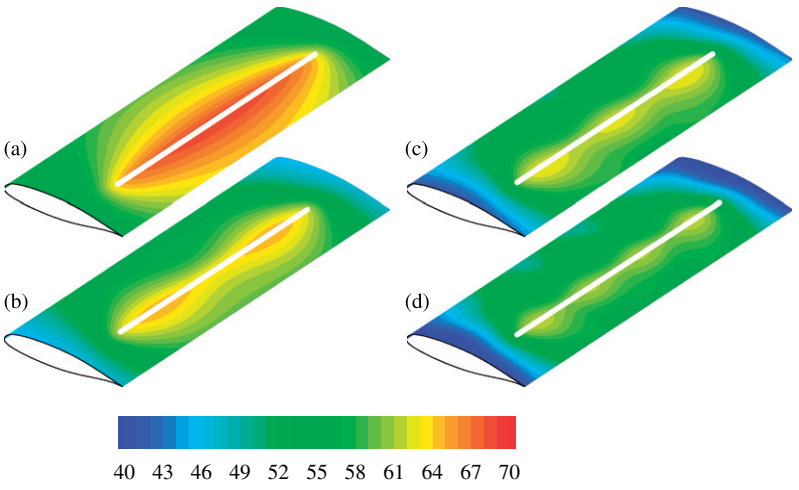

Fig. 9. Unsteady surface pressure amplitudes in dB generated by a uniform pulsed jet slot at the first five tonal frequencies: (a) $f = 217$ Hz; (b) $f = 651$ Hz; (c) $f = 1085$ Hz; and (d) $f = 1519$ Hz.

frequency is also demonstrated in Table 3, which lists the maximum values of the near-field pressure levels at the four tonal frequencies shown in Fig. 9.

For the four discrete frequencies shown in Fig. 9, the dependence of the pressure levels on the mean flow Mach number is shown in Fig. 10, which plots the pressure levels at the middle point between the actuator and the trailing edge on the symmetry line of the slot. For all the frequencies, the general trend is that the pressure levels increase with the flow Mach number, but the rate of increase is not uniform. The tone at the prime frequency shows the most increase in the Mach number range shown in this figure, and the increase becomes progressively gradual as the frequency increases. To illustrate the dependence of the pressure levels on the slot sizes, the pressure levels are plotted in Fig. 11 for the first four tones in the spectrum, as a function of the slot semi-span b for the same location as in Fig. 10. Interestingly, none of the tones show significant variations with the slot semi-span, when the length of the slot exceeds the airfoil chord. This is due to the fact that the dominant contributions to the pressure fluctuations in the near field are from the segments of the pulsed jet close to the microphone location. When the slot length increases, the contributions from the additional pulsed jet segments are small because they are far away from the microphone. It should be pointed out that for

Table 3
Maximum levels of the near field pressures at the four tones shown in Fig. 9

f (Hz)	217	615	1085	1519
SPL (dB)	68.7	64.9	63.0	61.7

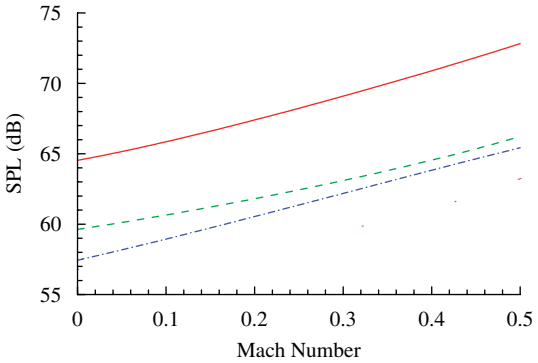

Fig. 10. Mach number dependence of the near-field pressure from a uniform slot pulsed jet. Solid curve $f = 217$ Hz; dashed curve $f = 651$ Hz; dash-dotted $f = 1085$ Hz; and dotted curve $f = 1519$ Hz.

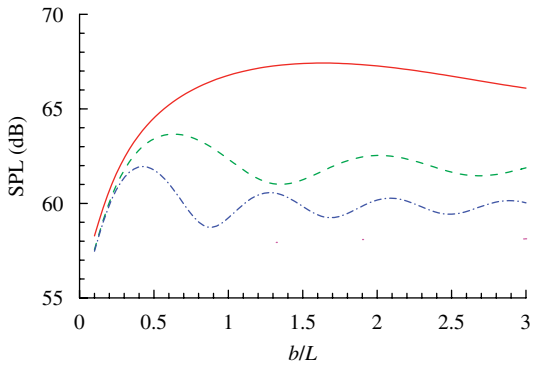

Fig. 11. Effect of actuator length on the near-field pressure from a uniform slot pulsed jet. Solid curve $f = 217$ Hz; dashed curve $f = 651$ Hz; dash-dotted $f = 1085$ Hz; and dotted curve $f = 1519$ Hz.

far-field microphones, contributions from all segment of the jet are comparable so that the far-field noise is proportional to the open area of the jet, as will be discussed in the following section.

5. Far-field noise

The far-field noise radiated by the pulsating jet actuators can be derived from the induced pressure Eq. (12) by utilizing the far-field condition

$$|\mathbf{x}| \gg |\mathbf{y}|. \tag{19}$$

This enables the expansion of the integrand of Eq. (12) in the form of inverse power of the far-field distance. The leading order term for the distance quantity is given by

$$R^* = |\mathbf{x}|\sqrt{\beta^2 + M^2\hat{x}_1^2}\left(1 - \frac{y_1\hat{x}_1 + \beta^2 y_2\hat{x}_2}{|\mathbf{x}|(\beta^2 + M^2\hat{x}_1^2)}\right), \tag{20}$$

where we have defined the mean flow velocity to be in the x_1 direction without loss of generality. The overhead hat in the far-field coordinates indicates components of the unit directional vector. When this expansion is substituted into the result Eq. (13), the second term inside the bracket, which is of second order in comparison with unity, is needed only in the phase function, which leads to

$$R^* + M(x_1 - y_1) = |\mathbf{x}|\left(\sqrt{\beta^2 + M^2\hat{x}_1^2} + M\hat{x}_1\right) - \frac{y_1\hat{x}_1 + \beta^2 y_2\hat{x}_2}{\sqrt{\beta^2 + M^2\hat{x}_1^2}} - My_1. \tag{21}$$

With this, result (13) simplifies to

$$G(\mathbf{x} - \mathbf{y}) = B(\mathbf{x})\,\mathrm{e}^{-\mathrm{i}\left(k_0/\beta^2\right)\left(\left(\left(y_1\hat{x}_1 + \beta^2 y_2\hat{x}_2\right)\Big/\sqrt{\beta^2 + M^2\hat{x}_1^2}\right) + My_1\right)}. \tag{22}$$

Here we have introduced B to save writing, which contains all quantities independent of $\mathbf{y}$ so that can be moved to the outside of the integration in Eq. (13). It is given by

$$B(\mathbf{x}) = \frac{\rho_0\omega}{2\pi\mathrm{i}\beta^2|\mathbf{x}|\sqrt{\beta^2 + M^2\hat{x}_1^2}}\left\{1 + \frac{M\hat{x}_1}{\sqrt{\beta^2 + M^2\hat{x}_1^2}}\right\}\mathrm{e}^{\mathrm{i}k_0|\mathbf{x}|\left(\sqrt{\beta^2 + M^2\hat{x}_1^2} + M\hat{x}_1\right)/\beta^2}. \tag{23}$$

By substituting all these into Eq. (12), the far-field sound pressure is then given by

$$\tilde{p}(\omega, \mathbf{x}) = V_J\tilde{F}(\omega)B(\mathbf{x})\int_{S(\mathbf{y})}\mathrm{e}^{-\mathrm{i}\omega\tau(\mathbf{y})}\,\mathrm{e}^{-\mathrm{i}\left(k_0/\beta^2\right)\left(\left(\left(y_1\hat{x}_1 + \beta^2 y_2\hat{x}_2\right)\Big/\sqrt{\beta^2 + M^2\hat{x}_1^2}\right) + My_1\right)}\,\mathrm{d}y_1\,\mathrm{d}y_2. \tag{24}$$

For pulsed jet actuators with continuous slots, the time delay is defined by Eq. (3). In this case, the remaining integrals in Eq. (24) can be carried out analytically with the result

$$\tilde{p}(\omega, \mathbf{x}) = 4bhV_J\tilde{F}(\omega)B(\mathbf{x})\,\mathrm{sinc}\left(\frac{k_0 h}{\beta^2}\frac{\hat{x}_1 + M}{\sqrt{\beta^2 + M^2\hat{x}_1^2}}\right)\mathrm{sinc}\left\{k_0 b\left(\eta + \frac{\hat{x}_2}{\sqrt{\beta^2 + M^2\hat{x}_1^2}}\right)\right\}, \tag{25}$$

where the sinc function is defined by the sine function divided by its argument, namely,

$$\mathrm{sinc}(x) = \sin(x)/x. \tag{26}$$

Similarly to the near-field pressure fluctuations discussed in the previous section, this result can be analyzed to reveal the dependencies of the far-field noise on various flow and geometric parameters, such as the flow Mach number and the jet slot dimensions. Though these results are only the direct radiation from the jet slot without the effects of reflection/diffraction by the airfoil, they can be regarded as the leading order contribution to the total noise, and the functional dependencies of the noise on the mean flow conditions and the pulsed jet conditions can be expected to hold for the total radiation. Similarly to the near-field pressure, the spectrum Eq. (25) is also dominated by sharp tones generated by the prime and harmonics of the jet flow, as is

clear from the proportionality of the jet velocity spectrum in Eq. (25). The mean flow Mach number dependence of the far-field noise is also similar to the near-field pressures discussed in the previous section. The general trend is that the amplitudes of the tones increase with the flow Mach number. This amplitude increase with flow Mach number is essentially due to the effects of flow convective amplification of the acoustic waves. The analytical results derived above shows that

$$\tilde{p}(\omega, \mathbf{x}) \sim 1/\beta^3 = (1 - M^2)^{-3/2} \tag{27}$$

which is a decreasing function of the mean flow mach number. Other parametric trends can also be extracted from the analytical results. It can be noted that the far-field noise increases with the size of the slot pulsed jet, which is given by Eq. (25) in the form of

$$\tilde{p}(\omega, \mathbf{x}) \propto bh. \tag{28}$$

This is different from the dependence of the near-field pressure analyzed in the previous section, where the near-field pressure does not show significant variations with the pulsed jet dimensions, because the dominant contributions to the near-field pressures come from the segments of the jet close to the measurement location. For the far-field noise, the jet dimensions are small compared with the distance of the microphones and all segments of the jet slot contribute to the far field almost equally. This is why the total far-field noise is proportional to the size of the slot. In addition to the tonal structure of the far-field noise determined by the jet velocity spectrum, there are also frequency variations due to other terms in result (25). As discussed in the previous section, the jet velocity spectrum is inversely proportional to frequency. This is offset by the frequency in the quantity B so that the frequency dependence of the far-field noise is determined by the two sinc functions in Eq. (25), which lead to

$$\tilde{p}(\omega, \mathbf{x}) \propto 1/\omega^2. \tag{29}$$

This is clearly different from the trend for the near-field pressure fluctuations, given by Eq. (27), and shows more rapid decrease of the tonal amplitudes with frequency. The far-field results also include the microphone locations, defined by $\mathbf{x}$, which leads to the far-field directivity of the radiated noise. Since the simple analytical results do not include the effects of the airfoil reflection/diffraction, this far-field directivity is only for the direct waves from the pulsed jets, but not the total radiation. Clearly, it is the explicit functional dependency of the far-field noise on the modulating parameter η that is of interest here. This dependency is given by the second sinc function in Eq. (25) and it controls the low noise design of the pulsed jet actuators. This is discussed in detail in the next section.

6. Low noise design

With the baseline case discussed in the previous sections for both the near-field pressure fluctuations and the far-field radiation, we will study in this section the low noise design of the pulsed jet actuators. As described early in the paper, the low noise design can be achieved by the spatially modulated time delay specified by Eqs. (2) and (4), respectively, for continuous and discrete array actuators. Since we have demonstrated by computational fluid dynamics simulation that actuations with time delays are as effective as uniform pulsation in flow control, it only remains to illustrate their low noise features. This will be done by comparing the surface pressure fluctuations and far-field noise levels with the baseline case of uniform pulsation.

We start with the surface pressure fluctuations, shown in Figs. 12 and 13, which plots the amplitudes of the unsteady surface pressures on the upper surface of the airfoil for various values of the modulation parameter η, respectively, at the jet pulsation frequency and its first harmonics, namely, the first two tones in the surface pressure spectrum. For comparison, the case with conventional pulsed jet of spatially uniform velocity distribution is also shown in these figures as the case of $\eta = 0$. The same level scales are used for all the cases to show clearly the comparison. To indicate how much lower the unsteady pressures are for the low noise design, the maximum values for each case are listed in Table 4. The flow and geometry conditions of the airfoil and the pulsed jet actuator are the same as those used in the numerical simulation discussed in earlier sections, as summarized in Tables 1 and 2. The results show that the spatially modulated actuators have significantly lower levels of surface pressure fluctuations and by suitably choosing the actuator design, the unsteady pressures can

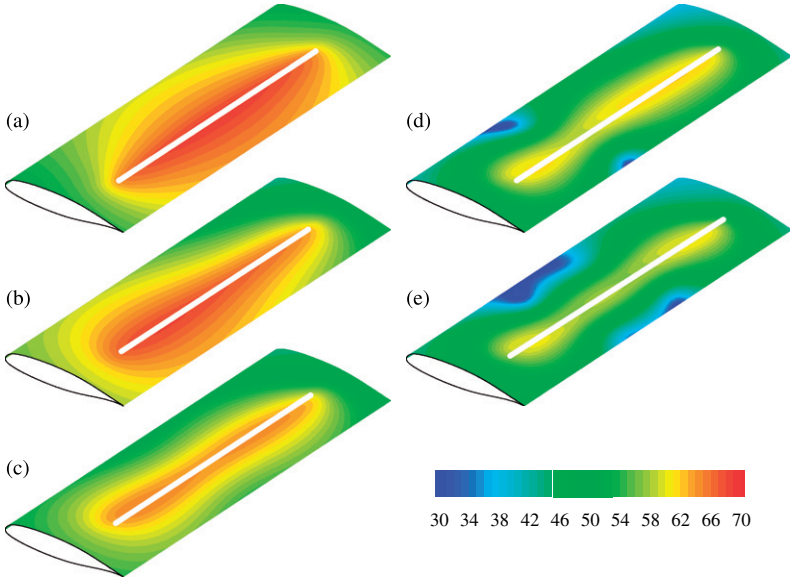

Fig. 12. Unsteady surface pressure amplitudes in dB due to a phased pulsating jet at its primary pulsation frequency: (a) $\eta = 0$; (b) $\eta = 1$; (c) $\eta = 2$; (d) $\eta = 3$; and (e) $\eta = 4$.

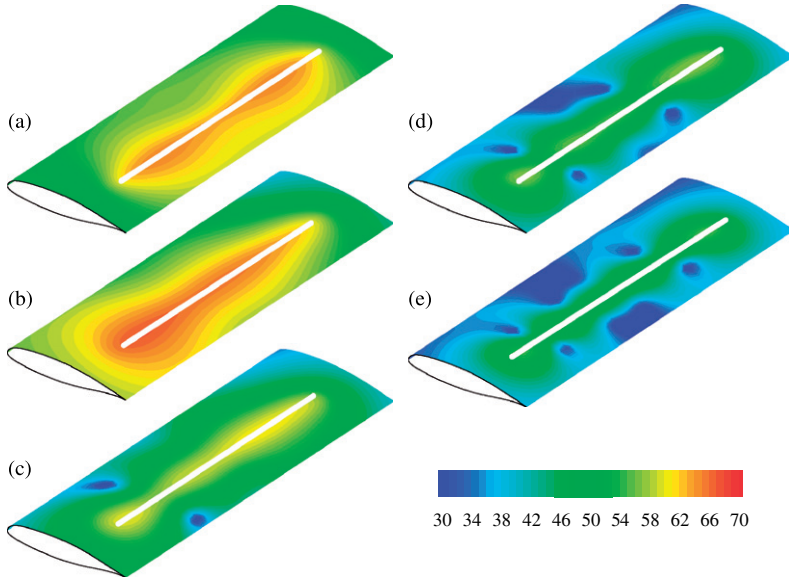

Fig. 13. Unsteady surface pressure amplitudes in dB due to a phased pulsating jet at its first harmonics: (a) $\eta = 0$; (b) $\eta = 1$; (c) $\eta = 2$; (d) $\eta = 3$; and (e) $\eta = 4$.

Table 4
Maximum levels of near field surface pressure fluctuations (in dB) shown in Figs. 12 and 13

η	0	1	2	3	4
1st tone	68.7	68.2	64.8	62.1	61.0
2nd tone	64.9	61.2	60.9	57.3	54.9

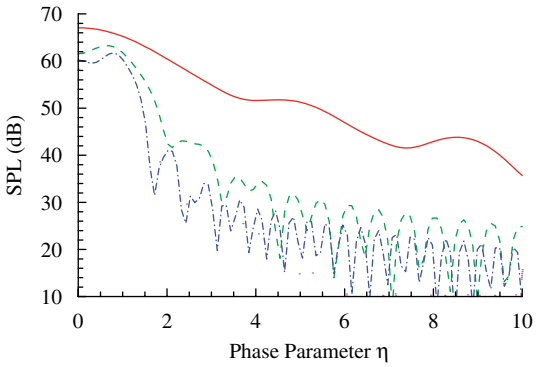

Fig. 14. Surface pressure levels as a function of the phase modulation parameter η for the first four tones. Solid curve $f = 217$ Hz; dashed curve $f = 651$ Hz; dash-dotted $f = 1085$ Hz; and dotted curve $f = 1519$ Hz.

be reduced to insignificant levels. These conclusions are further illustrated in Fig. 14, for the surface location that is at the middle point between the actuator and the trailing edge on the symmetry line of the slot length. The figure shows the pressure levels at this location for the first four tones in the spectrum as a function of the modulating parameter η, demonstrating the effectiveness of suppressing the surface pressures by phase modulation for all the tones.

For the far-field noise, the low noise features are characterized by the second sinc function in the result Eq. (25), from which, the effects of the phase modulation in the jet velocity pulsation can be defined as

$$\Delta = 20\log\left|\operatorname{sinc}\left\{\frac{2\pi mb}{c_0 T}\left(\eta + \frac{\sin\theta\sin\phi}{\sqrt{\beta^2 + M^2\sin^2\theta\cos^2\phi}}\right)\right\}\right|, \tag{30}$$

where we have rewritten the far-field microphone direction unit vector in terms of the polar angle θ and the azimuthal angle ϕ according to

$$\hat{x}_1 = \sin\theta\cos\phi \text{ and } \hat{x}_2 = \sin\theta\sin\phi. \tag{31}$$

We have also replaced the frequency by those at the discrete tones so that result (30) is for the tones, whose order is denoted by m. For slot design commonly used in active flow control, the slot width is usually small. The above result then shows that the low noise features are dominantly controlled by the slot length, defined by the slot semi-span b, the pulsating frequency as given by the inverse of the pulsation period T, and the phase modulation parameter η. The low noise design objective is then to suitably choose a combination of this set of parameters to achieve minimum noise. This can be done by numerically studying Eq. (30) or Eq. (25), or by constructing a cost function by integrating Eq. (25) to derive the total acoustic power radiated from the pulsed jet and finding the set of parameters by requiring minimum radiation.

For a simple analysis to demonstrate how low noise pulsed jet can be designed, we focus on the far-field location directly above the jet slot, which is also the maximum radiation direction. In this case, we set

$$\theta = 0 \text{ and } \phi = 0, \tag{32}$$

so that result (30) simplifies to

$$\Delta = 20\log\left|\operatorname{sinc}\frac{2\pi mb\eta}{c_0 T}\right|. \tag{33}$$

It is then clear that the radiation is zero if the argument of the sinc function is an integer multiple of π, namely, the quantity

$$m\eta(2b/c_0 T) \tag{34}$$

is an integer. Note that the quantity in the bracket is the ratio of the slot length to the acoustic wavelength at the pulsation frequency. For a given pulsed jet design, these two are defined to achieve the desired

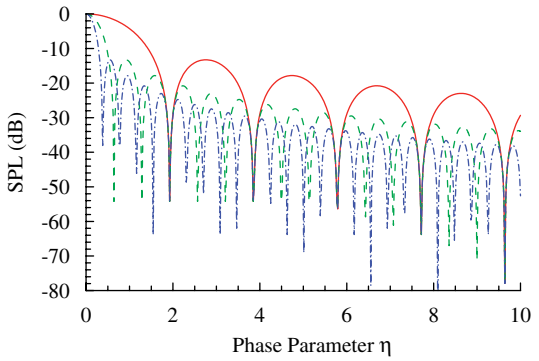

Fig. 15. Effect of phase modulation on far-field noise for the first three tones in the direction directly above the pulsed jet. Solid curve $f = 217$ Hz; dashed curve $f = 651$ Hz; and dash-dotted $f = 1085$ Hz.

aerodynamic performance so that the phase modulation parameter η can be chosen to make Eq. (34) close to an integer, which would lead to optimal low noise design. This optimal design may not always be feasible in practical applications, because of the practical constraints in the design and the potential needs to have low noise radiation for all tones and in all directions. It is important to note that because the linear phase cancellation mechanism is so strong that even if this condition is not satisfied, significantly low noise radiation can still be achieved. To demonstrate this, the result Eq. (33) is plotted in Fig. 15, as a function of the phase modulation parameter η for the first four tones in the noise spectrum. For this case, the ratio of the slot length to the acoustic wavelength at the jet pulsation frequency is 0.519. The results in Fig. 15 show that at some values of η, the radiation is almost zero, and the extremely low levels of far-field noise are for all tones. However, if these particular values cannot be chosen due to practical constraints, very low levels of radiation can still be achieved for other values of η, which makes the low noise design of pulsed jet actuators by phase modulation very robust.

7. Conclusion

In this paper, we have discussed the design of actuation strategies for active flow control, from the acoustics point of view, with emphasis on designs that lead to both low induced near-field pressure fluctuations and low far-field noise radiation. The study has been motivated by the potential risks of pulsed jet induced acoustic fatigue and noise pollution; aeroacoustic loads on structures due to pulsed jet actuators may be significant because the prime pulsating frequency is usually low and within the range of structural resonance frequencies, and the far-field noise may be a potential environmental issue because of the rich content of harmonics in pulsed jet velocities commonly used in active flow control, which may generate sharp tones in the far-field noise with frequencies within the domain for human ear reception. To mitigate these risks, we have demonstrated that spatially modulated time delays in the pulsed jet velocity can achieve significantly low near-field pressure and far-field noise levels, in comparison with the case of spatially uniform pulsation. For the particular example of flow separation control on airfoils, we have shown that the low noise design is as effective as actuators with uniform pulsation. To help with practical applications, the aeroacoustics analysis has been done in simple analytical forms, with approximations justified by the flow and geometric conditions of the flow separation control example. Simple analytical results have been derived that relate the radiated noise to flow and design parameters, which can be used as a quick guideline in practical applications of actuator strategy design. It should be noted that for applications different from airfoil flow separation control, more detailed aeroacoustic analysis may be needed to design control strategies that are effective both in flow control and low noise radiation, and robust for practical applications. The level of details in the analysis will apparently depend on the flow and geometric conditions of the particular applications, but the study reported here has clearly established the principles of designing the control strategies to achieve the dual objective.

Acknowledgments

The author would like to thank Dr. Feng Jiang of the Boeing Company for her help in obtaining the computational fluid dynamics simulations discussed in this paper and for many helpful general discussions on computational fluid dynamics and active flow control.

References

[1] S. Anders, W. Sellers III, A. Washburn, Active flow control activities at NASA Langley, Paper presented at the *Second AIAA Flow Control Conference*, Portland, OR, USA, 28 June–1 July 2004, AIAA Paper 2004-2623, 2004.
[2] W. Bower, V. Kibens, An overview of active flow control applications at The Boeing Company, Paper presented at the *Second AIAA Flow Control Conference*, Portland, OR, USA, 28 June–1 July 2004, AIAA Paper 2004-2624, 2004.
[3] Ronald D. Joslin, Lucas G. Horta, Fang-Jenq Chen, Transitioning active flow control to applications, Paper presented at the *30th AIAA Fluid Dynamics Conference*, Norfolk, VI, USA, 28 June–1 July, 1999, AIAA Paper 1999-3575, 1999.
[4] M.P. Patel, A.B. Cain, Numerical simulation of flow control techniques for separation control, Paper presented at the *40th AIAA Aerospace Sciences Meeting and Exhibit*, Reno NV, USA, January 14–17, 2002, AIAA Paper 2002-0668, 2002.
[5] A. Stalker, D. Cerchie, L. Cullen, I. Wygnanski, Using periodic perturbations for download alleviation on tilt-rotor airplane models in Hover, Paper presented at *Second AIAA Flow Control Conference*, Portland, OR, USA, 28 June–1 July 2004, AIAA Paper 2004-2515, 2004.
[6] B. Allan, L. Owens, B. Berrier, Numerical modeling of active flow control in a boundary layer ingesting offset inlet, Paper presented at *Second AIAA Flow Control Conference*, Portland, OR, USA, 28 June–1 July 2004, AIAA Paper 2004-2318, 2004.
[7] Michael Hites, Hassan Nagib, Tomer Bachar, Israel Wygnanski, Enhanced performance of airfoils at moderate Mach numbers using zero-mass flux pulsed blowing, *39th Aerospace Sciences Meeting; Exhibit*, Reno, NV, USA, 12–15 January 2001, AIAA Paper 2001-0734, 2001.
[8] J.E. Ffowcs Williams, Active flow control, *Journal of Sound and Vibration* 239 (4) (2001) 861–871.
[9] N. Peake, D.G. Crighton, Active control of sound, *Annual Review of Fluid Mechanics* 32 (2000) 137–164.
[10] Ronald D. Joslin, Russell H. Thomas, Meelan M. Choudhari, Synergism of flow and noise control technologies, *Progress in Aerospace Sciences* 41 (2005) 363–417.
[11] P. Joseph, C.L. Morfey, P.A. Nelson, Active control of source sound power radiation in uniform flow, *Journal of Sound and Vibration* 212 (2) (1998) 357–364.
[12] F. Jiang, Computational analyses for an advanced propeller powered theater transport, Paper presented at the *21st Applied Aerodynamics Conference*, Orlando, FL, USA, 23–26 June 2003, AIAA Paper 2003-4081, 2003.
[13] D. Manley, W. von Klein, Design and development of a super short takeoff and landing transport aircraft, *2002 Biennial International Powered Lift Conference and Exhibit*, Williamsburg, VI, USA, 5–7 November 2002, AIAA Paper 2002-6023, 2002.
[14] M.S. Howe, Noise generation by a coanda wall jet circulation control device, *Journal of Sound and Vibration* 249 (4) (2002) 679–700.
[15] P.W. Carpenter, C. Smith, The aeroacoustics and aerodynamics of high-speed coanda device, part 2: effects of modifications for flow control and noise reduction, *Journal of Sound and Vibration* 208 (5) (1997) 803–822.
[16] P.M. Morse, K.U. Ingard, *Theoretical Acoustics*, McGraw-Hill, New York, 1968.